

Article

Binary Neutron Star Merger Simulations with a Calibrated Turbulence Model

David Radice^{1,2,3} ¹ Institute for Gravitation & the Cosmos, The Pennsylvania State University, University Park, PA 16802² Department of Physics, The Pennsylvania State University, University Park, PA 16802³ Department of Astronomy & Astrophysics, The Pennsylvania State University, University Park, PA 16802Version November 2, 2021 submitted to *Symmetry*

Abstract: Magnetohydrodynamic (MHD) turbulence in neutron star (NS) merger remnants can impact their evolution and multimessenger signatures, complicating the interpretation of present and future observations. Due to the high Reynolds numbers and the large computational costs of numerical relativity simulations, resolving all the relevant scales of the turbulence will be impossible for the foreseeable future. Here, we adopt a method to include subgrid-scale turbulence in moderate resolution simulations by extending the large-eddy simulation (LES) method to general relativity (GR). We calibrate our subgrid turbulence model with results from very-high-resolution GRMHD simulations, and we use it to perform NS merger simulations and study the impact of turbulence. We find that turbulence has a quantitative, but not qualitative impact on the evolution of NS merger remnants, on their gravitational wave signatures, and on the outflows generated in binary NS mergers. Our approach provides a viable path to quantify uncertainties due to turbulence in NS mergers.

Keywords: Gravitational Waves; Nuclear Astrophysics; Hydrodynamics

1. Introduction

Binary neutron star (BNS) mergers are prime targets for the ground-based laser interferometric gravitational-wave (GW) detectors LIGO [1], Virgo [2], and KAGRA [3]. BNS mergers generate loud GW signals and can also power bright electromagnetic (EM) transients [4–10], as demonstrated by the extraordinary multimessenger observations of GW170817 [11,12]. Finally, BNS mergers can eject neutron rich material which subsequently produces heavy elements, such as gold and uranium, through the r-process [4,13–15]. At the time of writing, one more BNS GW event after GW170817 has been announced by the LIGO/Virgo collaboration (LVC): GW190425 [16,17]. However, several more candidates have been reported and are currently being analyzed by the LVC [18]. Many more detections are expected in the next years as GW observatories improve their sensitivities and as more facilities are added to the global network of detectors [19].

Multimessenger observations of BNS mergers are starting to constrain the poorly known properties of matter at extreme densities [11,12,20–36] and the physical processes powering short γ -ray bursts (SGRBs) [37–42]. They are also beginning to reveal the role played by compact binary mergers in the chemical enrichment of the galaxy with r-process elements [8,13,43–62]. The key to the solution of some of the most pressing open problems in nuclear and high-energy astrophysics – such as the origin of heavy elements, the nature of neutron stars (NSs), and the origin of SGRBs – is encoded in these and future observations. However, theory is essential to turn observations into answers.

Numerical relativity (NR) simulations are the only tool able to study the dynamics of BNS mergers in the strong field regime and its connection to the multimessenger signals they produce. State-of-the-art NR simulations include a microphysical treatment of dense matter, the impact of weak reactions and neutrino radiation, and magnetic effects [63–66]. Even though modern simulations ostensibly include all of the physics believed to determine the outcome of BNS mergers, the long-term evolution of binaries after merger remains poorly known, *e.g.*, [67]. Leading sources of uncertainty are connected to our limited knowledge of the behavior of matter at extreme densities and temperatures, the crudeness with which neutrino radiation is treated in the simulations, and our inability to simulate these systems at sufficiently high resolution to resolve the turbulent cascade and for sufficiently long times [68]. This work is part of our ongoing effort to address this last issue.

It is known that the matter flow after merger is subject to a number of magnetohydrodynamics (MHD) instabilities, such as the Kelvin-Helmholtz (KH) instability and the magnetorotational instability (MRI) [69–75]. These inject turbulence at very small scale and can potentially impact the qualitative outcome of the merger [76–79]. However, even the best resolved GRMHD simulations to date [65,74,75] cannot capture the scale of the fastest growing mode of the MRI, unless artificially large initial magnetic fields are adopted to increase the cutoff length scales associated with some of these instabilities. Even in these cases, simulations are far from being able to capture the dynamics of the turbulent cascade all the way to the viscous scale, at which neutrino viscosity and drag damps the turbulent eddies [80], as would be required for a DNS simulation.

In Ref. [81] we proposed the general-relativistic large-eddy simulation (GRLES) method as an alternative to performing ultra-high resolution GRMHD simulations. In particular, we proposed to evolve the coarse-grained GRHD equations with a turbulent closure models design to capture the effect of turbulence operating at sub-grid scales. In parallel, a similar, but technically distinct, approach based on the Israel-Stewart formalism was proposed by Shibata and collaborators [82]. More recently, a rigorous first-principle theory of relativistic turbulence that, among other things, strengthens the mathematical foundation for the GRLES method, has been proposed by Eyink and Drivas [83]. An extension of the method to GRMHD, taking into account also terms that we neglected in our initial formulation (more on this below), has been proposed in Refs. [84,85]. Rosofsky and Huerta [86] proposed to use machine learning to calibrate subgrid turbulence models for 2D MHD. Finally, a variant of the GRLES method has also been implemented into the SpEC code by the SXS collaboration to perform 2D axisymmetric simulations [66].

The GRLES or viscous approaches are the only way to perform long-term simulations of the postmerger evolution for multiple systems [56,61,62]. However, the results from these simulations inevitably depend on the adopted subgrid model. In earlier work we used turbulence models based on dimensional analysis and linear perturbation theory. Here, we calibrate a subgrid model using results from very high resolution GRMHD simulations performed by Kiuchi and collaborators [75], which were able to resolve all the unstable scales of the MRI for a binary system with an initially large magnetic field. We perform BNS merger simulations with microphysics and compare results obtained with the newly calibrated turbulence model with those obtained using the prescription we proposed in Ref. [81], which was used in several other works [58,61,87–90], and to those obtained with traditional GRHD simulations having no subgrid model. We find that turbulence can impact the postmerger evolution of BNSs in a quantitative way, and we discuss the implications for the interpretation of synthetic GW, EM, and nucleosynthesis yields from BNS merger simulations.

The rest of this paper is organized as follows. In Section 2 we review the GRLES formalism and discuss the calibration of the subgrid model. In Section 3 we present our simulation results. Finally, Section 4 is dedicated to discussion and conclusions.

2. Methods

2.1. WhiskyTHC

All simulations are performed with the WhiskyTHC code [91–94]. WhiskyTHC separately evolves the proton and neutron number densities

$$\nabla_{\mu}(J_{p,n}^{\mu}) = R_{p,n}, \quad (1)$$

where $J_{p,n}^{\mu} = n_{p,n}u^{\mu}$ are the proton and neutron four-currents, $n_p = Y_e n$ is the proton number density, n_n is the neutron number density, $n = n_p + n_n$ is the baryon number density (including baryons in nuclei), u^{μ} the fluid four-velocity, and Y_e is the electron fraction of the material. $R_p = -R_n$ is the net lepton number deposition rate due to the absorption and emission of neutrinos and anti-neutrinos, which is computed using the M0 scheme [50,58].

NS matter is treated as a perfect fluid with stress energy tensor

$$T_{\mu\nu} = (e + p)u_{\mu}u_{\nu} + pg_{\mu\nu}, \quad (2)$$

where e is the energy density and p the pressure. We solve the equations for the balance of energy and momentum

$$\nabla_{\nu}T^{\mu\nu} = Qu^{\mu}, \quad (3)$$

where Q is the net energy deposition rate due to the absorption and emission of neutrinos, also treated using the M0 scheme.

The spacetime is evolved using the Z4c formulation of Einstein's equations [95,96] as implemented in the CTGamma code [97,98], which is part of the Einstein Toolkit [99,100]. CTGamma and WhiskyTHC are coupled using the method of lines. For this work we use the optimal strongly-stability preserving third-order Runge-Kutta scheme [101] as time integrator. Mesh adaptivity is handled using the Carpet mesh driver [102] which implements Berger-Oliger style adaptive mesh refinement (AMR) with subcycling in time and refluxing [103–105].

2.2. GRLES

According to the Valencia formalism for GRHD [106] the fluid four-velocity is decomposed as the sum of a vector parallel and one orthogonal to the $t = \text{const}$ hypersurface normal n^{μ} (not to be confused with the neutron and proton number densities) as:

$$u^{\mu} = (-u_{\mu}n^{\mu})(n^{\mu} + v^{\mu}) =: W(n^{\mu} + v^{\mu}), \quad (4)$$

where W is the Lorentz factor and v^{μ} is the three velocity. Accordingly, the proton and neutron currents can be written as

$$J_{n,p}^{\mu} = n_{n,p}W(n^{\mu} + v^{\mu}) =: D_{n,p}(n^{\mu} + v^{\mu}). \quad (5)$$

In a similar way, the stress energy tensor is decomposed as

$$T_{\mu\nu} = En_{\mu}n_{\nu} + S_{\mu}n_{\nu} + S_{\nu}n_{\mu} + S_{\mu\nu}, \quad (6)$$

where

$$E = T_{\mu\nu}n^\mu n^\nu = (e + p)W^2 - p, \quad (7)$$

$$S_\mu = -\gamma_{\mu\alpha}n_\beta T^{\alpha\beta} = (e + p)W^2 v_\mu, \quad (8)$$

$$S_{\mu\nu} = \gamma_{\mu\alpha}\gamma_{\nu\beta}T^{\alpha\beta} = S_\mu v_\nu + p\gamma_{\mu\nu}, \quad (9)$$

are respectively the energy density, the linear momentum density, and the stress tensor in a frame having four-velocity n^μ , and $\gamma_{\mu\nu}$ is the spatial metric.

With these definitions in place, and neglecting the neutrino source terms to keep the notation simple, the GRHD equations read

$$\partial_t(\sqrt{\gamma}D_{n,p}) + \partial_j[\alpha\sqrt{\gamma}(v^j + n^j)D_{n,p}] = 0, \quad (10)$$

$$\partial_t(\sqrt{\gamma}S_i) + \partial_j[\alpha\sqrt{\gamma}(S_i^j + S_i n^j)] = \alpha\sqrt{\gamma}\left(\frac{1}{2}S^{jk}\partial_i\gamma_{jk} + \frac{1}{\alpha}S_k\partial_i\beta^k - E\partial_i\log\alpha\right), \quad (11)$$

$$\partial_t(\sqrt{\gamma}E) + \partial_j[\alpha\sqrt{\gamma}(S^j + E n^j)] = \alpha\sqrt{\gamma}(K_{ij}S^{ij} - S^i\partial_i\log\alpha). \quad (12)$$

The GRLES methodology derives a set of equations for the large scale dynamics of the flow, in the sense precisely defined in Ref. [83], by applying a linear filtering operator $X \mapsto \bar{X}$ to derive a set of equations for the coarse grained quantities. For example, the cell averaging done in the context of a finite volume method can be considered as a type of filtering. The averaged equations read:

$$\partial_t(\sqrt{\gamma}\overline{D_{n,p}}) + \partial_j[\alpha\sqrt{\gamma}(\overline{D_{n,p}v^j} + \overline{Dn^j})] = 0, \quad (13)$$

$$\partial_t(\sqrt{\gamma}\overline{S_i}) + \partial_j[\alpha\sqrt{\gamma}(\overline{S_i^j} + \overline{S_i n^j})] = \alpha\sqrt{\gamma}\left(\frac{1}{2}\overline{S^{jk}}\partial_i\gamma_{jk} + \frac{1}{\alpha}\overline{S_k}\partial_i\beta^k - \overline{E}\partial_i\log\alpha\right), \quad (14)$$

$$\partial_t(\sqrt{\gamma}\overline{E}) + \partial_j[\alpha\sqrt{\gamma}(\overline{S^j} + \overline{E n^j})] = \alpha\sqrt{\gamma}(K_{ij}\overline{S^{ij}} - \overline{S^i}\partial_i\log\alpha). \quad (15)$$

Here, we have implicitly assumed that the metric quantities are unaffected by averaging, because they are already large scale quantities. This is the only approximation made when going from Eqs. (10)-(12) to Eqs. (13)-(15). Although these equations can be considered exact, they are obviously not closed, since not all terms can be expressed solely as a function of the evolved quantities $\overline{D_{n,p}}$, $\overline{S_i}$, and \overline{E} . This is a manifestation of the nonlinearity of the equations. To close the equations it is necessary to provide a closure for some of the terms. The most obvious terms that need to be closed are the quadratic terms:

$$\overline{S_{ij}} = \overline{S_i}\overline{v_j} + \overline{p}\delta_{ij} + \tau_{ij}, \quad \overline{Dv^i} = \overline{D}\overline{v^i} + \mu^i, \quad (16)$$

The correlation terms τ_{ij} and μ^i are the subgrid-scale, or turbulent, stress and rest-mass diffusion. We remark that these terms are always present in any numerical discretization of the GRHD equations even if not explicitly included: this is the so-called implicit large-eddy simulation (ILES) approach.

Since the equation of state (EOS) is also non-linear, the filtered pressure is not equal to the EOS evaluated from the coarse-grained quantities, so an additional closure would also be needed when evaluating \overline{p} , that is:

$$\overline{p} = p(\overline{D_{n,p}}, \overline{S_i}, \overline{E}) + \Pi \quad (17)$$

Similarly, the three velocity $\overline{v^i}$ is also a nonlinear function of the evolved coarse-grained quantities, so we would need to include a closure also for $\overline{v^i}$. These terms are treated in full generality in Refs. [84,85], to which we refer for the details. Here, we neglect these corrections, *e.g.*, we assume $\Pi = 0$, because we

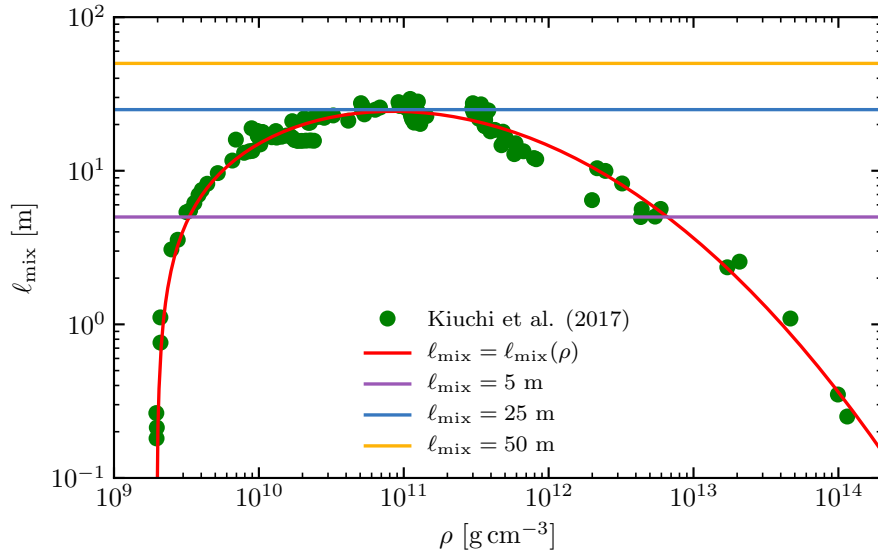


Figure 1. Mixing length evaluated from the GRMHD simulations of Kiuchi et al. [75] (dots) and fit employed in this work (red line). Also shown are the other values of ℓ_{mix} employed in this and in our previous works. GRMHD simulations favor relatively small values ℓ_{mix} in agreement with the simple analytic estimate in Eq. (20).

expect them to be subdominant, since turbulence in the postmerger remnant is subsonic and subrelativistic, meaning that its character should be fully captured by τ_{ij} . This assumption could in principle be verified using GRMHD simulation data. However, the simulations data that we use for calibration [75] is not publicly available, and we only have access to the value of the α parameter, which maps to $\tau_{r\phi}$. Consequently, we cannot check the validity of this assumption.

We employ the relativistic extension of the classical turbulence closure of Smagorinsky [107], which we proposed in Ref. [81]:

$$\tau_{ij} = -2\nu_T(e + p)W^2 \left[\frac{1}{2}(D_i\bar{v}_j + D_j\bar{v}_i) - \frac{1}{3}D_k\bar{v}^k\gamma_{ij} \right], \quad \mu^i = 0, \quad (18)$$

where D_i is the covariant derivative associated with γ_{ij} , and ν_T , the turbulent viscosity. On the basis of dimensional analysis arguments it is natural to parametrize ν_T in terms of a characteristic velocity, the sound speed c_s , and a characteristic length scale of turbulence, the mixing length ℓ_{mix} , as

$$\nu_T = \ell_{\text{mix}} c_s. \quad (19)$$

For MRI-driven turbulence, one can assume ℓ_{mix} to be related to the length scale of the most unstable mode of the MRI [77]

$$\lambda_{\text{MRI}} \sim 20 \text{ m} \left(\frac{\Omega}{6 \text{ rad ms}^{-1}} \right)^{-1} \left(\frac{B}{10^{15} \text{ G}} \right), \quad (20)$$

which is the scale at which turbulence is predominantly driven according to linear theory. Accordingly, in our previous work we explored the impact of turbulence by varying ℓ_{mix} between 0 and 50 m respectively corresponding to no and very efficient turbulent mixing.

In the context of accretion disk theory, turbulent viscosity is typically parametrized in terms of a dimensionless constant α linked to ℓ_{mix} through the relation $\ell_{\text{mix}} = \alpha c_s \Omega^{-1}$, where Ω is the angular

velocity of the fluid [108]. Recently, Kiuchi and collaborators [75] performed very high resolution GRMHD simulations of a NS merger with sufficiently high seed magnetic fields (10^{15} G) to be able to resolve the MRI in the merger remnant and reported averaged α values for different rest-mass density shells. Combining their estimate of α with values of c_s and Ω estimated from a simulation performed with $\ell_{\text{mix}} = 0$ we are able to estimate ℓ_{mix} as a function of the rest mass density (Fig. 1). We find that the mixing length is well fitted by the expression

$$\ell_{\text{mix}} = \begin{cases} a \zeta \exp(-|b \zeta|^{5/2}) \text{ [m]}, & \text{if } \zeta > 0, \\ 0, & \text{otherwise,} \end{cases} \quad (21)$$

where

$$\zeta = \log_{10} \left(\frac{m_b (n_p + n_m)}{\rho^*} \right), \quad (22)$$

m_b is the atomic mass unit in grams, $a = 22.31984$, $b = -0.4253832$, and $\rho^* = 1.966769 \times 10^9 \text{ g cm}^{-3}$. This fit and the constant values of ℓ_{mix} used in our previous studies, are shown in Fig. 1.

Our analysis reveals that ℓ_{mix} is relatively small even for the highly-magnetized binary considered by Kiuchi et al. [75]. The peak value of ℓ_{mix} estimated from the GRMHD simulations is remarkably close to the analytic prediction given by Eq. (20). We also find that the turbulence weakens at high densities inside the massive NS (MNS) product of the merger. This is expected, because the angular velocity deep inside the remnant grows with radius stabilizing the flow against the MRI [81,109–112]. On the other hand, the drop of ℓ_{mix} at low density is an artifact of our fitting procedure. Since Kiuchi et al. [75] do not provide the value of α for densities below $10^{10} \text{ g cm}^{-3}$ we perform a log-linear extrapolation of α to lower density which results in α becoming zero at the density ρ^* . That said, the value of ℓ_{mix} at those densities is inconsequential for our simulations, because the orbital period for the part of the disk with density ρ^* is comparable to the total postmerger simulation time. Overall, we find that turbulence is strongest in the mantle of the MNS and in the inner part of the disk, at densities between a few times 10^9 g cm^{-3} to $10^{13} \text{ g cm}^{-3}$.

2.3. Models and Simulation Setup

We consider a BNS system with component masses (at infinite separation) $M_A = M_B = 1.35 M_\odot$. The LS220 EOS [113] is used to describe the nuclear matter. The initial data is constructed with the Lorene code [114], while the evolution is performed with `WhiskyTHC` using the setup discussed in Ref. [58]. We simulate the same binary multiple times: once with the calibrated ℓ_{mix} from Sec. 2.2, and then with fixed constant values for ℓ_{mix} : 0, 5 m, 25 m, and 50 m. Additionally, each configuration is run twice: with and without the inclusion of neutrino reabsorption in the simulations. Neutrino cooling is instead always included. The resolution in the finest refinement level of the grid, which covers the NSs during the inspiral and the MNS after merger, is of 185 m. Finally, to quantify finite-resolution effects we also rerun the simulations with no neutrino reabsorption also at the lower resolution of 246 m. The results presented here are thus based on a total of 15 simulations for a total cost of about 3M CPU hours. The simulations with constant ℓ_{mix} were already presented¹ in Refs. [58,81,88]. In Ref. [65] postmerger profiles from the $\ell_{\text{mix}} = 0$ no neutrino reabsorption binary was mapped into a high-resolution grid and simulated with the inclusion of a magnetic field. The simulations with calibrated turbulence model are new. For clarity, we

¹ However, we rerun the $\ell_{\text{mix}} = 0$ simulation with neutrino reabsorption, which we now continue for a longer time after merger than in our previous work.

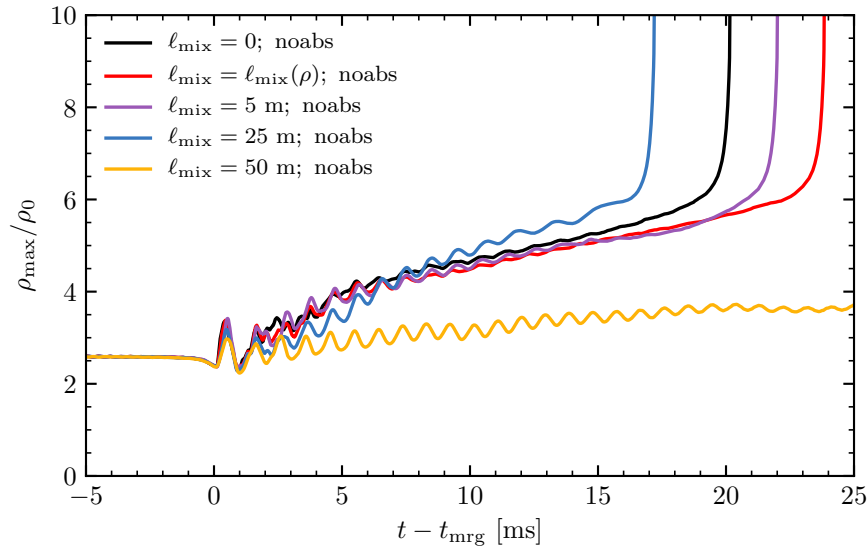


Figure 2. Maximum density evolution for the models computed without neutrino heating. We use nuclear saturation density ($\rho_0 = 2.7 \times 10^{14} \text{ g cm}^{-3}$) as density scale. The inclusion of turbulent viscosity can drastically alter the lifetime of the MNS.

only include the high-resolution simulations in the figures. If not otherwise specified, the figures refer to the simulations that included both neutrino emission and neutrino reabsorption. The low-resolution data follows the same qualitative trends, although there are quantitative differences.

3. Results

3.1. Qualitative Dynamics

We refer to Refs. [58,115] for a detailed description of the qualitative evolution of the binary considered in this work. Here, we only mention that the simulations span the last ~ 3 –4 orbits prior to merger and continue for 20–25 ms afterwards. The merger produces a MNS remnant that collapses to black hole (BH) surrounded by a massive accretion torus, typically within the simulation time. Notable exceptions are the simulations with $\ell_{\text{mix}} = 50$ m for which collapse appears to be significantly delayed by viscosity, as we reported in Ref. [81].

The evolution of the maximum rest-mass density for the 5 binaries that did not include neutrino heating is shown in Fig. 2. As previously reported in Ref. [81], we find that the turbulence on the lifetime of the remnant is non monotonic. This is due to the complex interplay between angular momentum transport and suppression of angular momentum losses to GWs operated by the turbulence [81]. However, only the simulation with the largest mixing length ($\ell_{\text{mix}} = 50$ m), corresponding to very efficient turbulent transport, shows truly significant differences in the contraction rate and in the lifetime of the remnant when compared to the baseline model with $\ell_{\text{mix}} = 0$. In the other cases the changes are quantitative rather than qualitative. This is not surprising: turbulent viscosity plays a small role in the inner core of the MNS because the velocity gradients are relatively small towards the center of the MNS [109–111]. These findings are consistent with the results of the GRMHD simulations of the same binary presented in Ref. [65]. There it was found that the inclusion or omission of the magnetic field (and hence of the MRI-induced turbulence) has a modest effect on the collapse time of the remnant, with difference of the same order as those found in our Fig. 2.

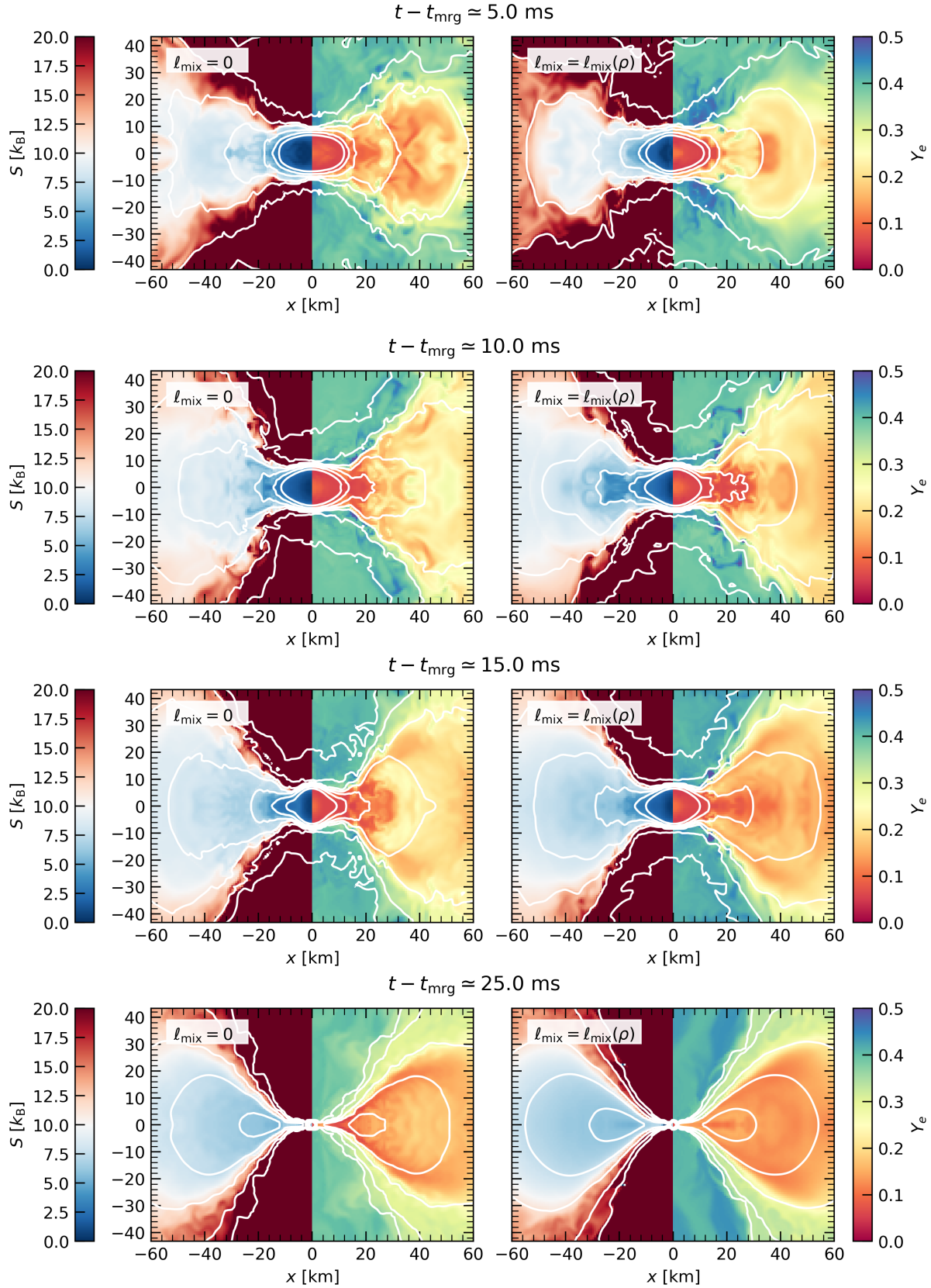


Figure 3. Remnant disk and MNS in the $\ell_{\text{mix}} = 0$ and $\ell_{\text{mix}} = \ell_{\text{mix}}(\rho)$ models at four representative times. In each panel we show color-coded values of entropy ($x < 0$) and electron fraction ($x > 0$) in the meridional plane. The bottom panel shows the disk configuration at the end of the simulation, when the MNS has collapsed to BH. The white lines are the $10^8, 10^9, 10^{10}, 10^{11}, 10^{12}, 10^{13}$, and $10^{14} \text{ g cm}^{-3}$ isocontours of the rest-mass density. Turbulent viscosity mixes material from the mantle of the MNS and the inner disks and smooths the structure of the disk.

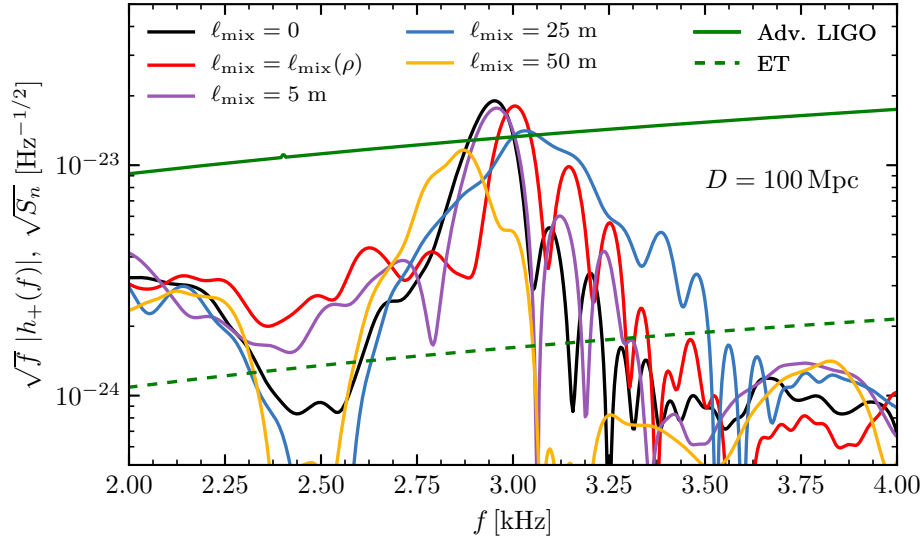


Figure 4. Effective strain the frequency domain for the dominant $\ell = 2, m = 2$ GW multipole for selected models. We window the GW strain data using an Hann window on the interval $-10 \text{ ms} < t - t_{\text{mrg}} < 20 \text{ ms}$. We show the effective strain for an optimally oriented binary at $D = 100 \text{ Mpc}$. Also shown are the design noise curves for Adv. LIGO, in the high laser power zero detuning configuration, and the Einstein Telescope, in the ET-D configuration. The effective strain is normalized so that the ratio between the signal and the noise curve is equal to the signal to noise ratio density in frequency space. Turbulent viscosity results in only modest shifts of the dominant postmerger emission frequency. However, the subdominant features in the GW spectrum are strongly impacted.

The effects of turbulent viscosity are more pronounced in the outer layers of the MNS and in the disk, where velocity gradients are larger. Moreover, ℓ_{mix} is maximum in this region according to the calibrated turbulence model. The impact of turbulence on the structure of the disk is shown in Fig. 3, where we report the profiles of entropy, electron fraction, and density for the $\ell_{\text{mix}} = 0$ and $\ell_{\text{mix}} = \ell_{\text{mix}}(\rho)$ runs (both with neutrino absorption included). The accretion disk is formed in the first milliseconds after the merger, as hot material is expelled from the collisional interface between the NSs. During this phase, turbulence dissipation enhances the thermalization of the flow resulting in the formation of a disk with larger initial entropy and electron fraction compared to that of the baseline model with $\ell_{\text{mix}} = 0$. At later times, turbulence has an opposite effect: turbulent stresses drive the mixing of the hot material in the inner disk with fresh low-entropy material from the mantle of the MNS lowering entropy and electron fraction in the inner part of the disk. Over longer timescales, turbulent angular momentum transport also drives flows of matter to larger radii. This manifests itself in the increase of the density in the midplane of the disk and the smoothing of the isodensity contours in the disk. We remark once again that the internal structure of the remnant is not visibly affected by the turbulence viscosity (with the exception of the $\ell_{\text{mix}} = 50 \text{ m}$ run). The apparent differences in the density isocontours in the MNS in Fig. 3 arise because the MNS has a strong quadrupolar deformation and the $\ell_{\text{mix}} = 0$ and $\ell_{\text{mix}} = \ell_{\text{mix}}(\rho)$ simulations are dephased with respect to each other.

3.2. Gravitational Waves

The impact of turbulent viscosity on the GW signal is shown in Fig. 4. The most prominent feature of the postmerger spectrum is a peak at $f_{\text{GW}} \simeq 3 \text{ kHz}$ associated with the rotational period of the

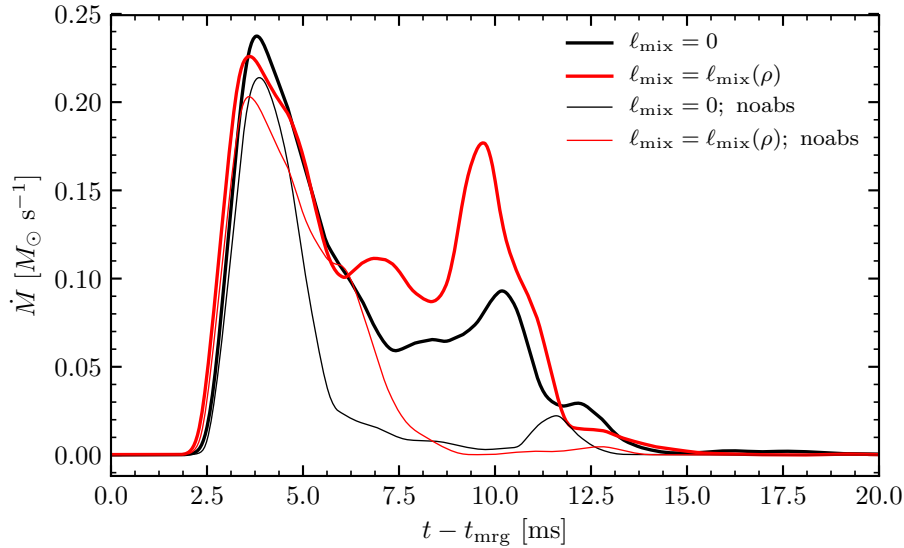


Figure 5. Outflow rate for the baseline and the calibrated turbulence models. The thin lines denote simulations that did not include neutrino reabsorption. For clarity we smooth the data using a rolling average with amplitude 0.5 ms. Turbulent dissipation has a modest impact on the dynamical ejecta mass and is subdominant in comparison to neutrino heating.

quadrupolarly deformed MNS [78,116–118]. We find this feature to be robust against turbulence: deviations in the peak frequency with ℓ_{mix} are typically small and of the same order of the nominal uncertainty of the Fourier transform of the time domain data. Thus, our results confirm that the measurement of the postmerger peak frequency is a promising avenue to constrain the EOS of dense matter using 3rd generation detectors, *e.g.*, Ref. [119]. Models with turbulent viscosities larger than those of our calibrated model, *i.e.*, $\ell_{\text{mix}} = 25$ m and $\ell_{\text{mix}} = 50$ m, also show an overall decrease in the power of the GW signal, suggesting that turbulence might suppress GW emission, as also found in Refs. [81,120]. That said, significant reduction in the GW signal as found by Ref. [120] would require turbulent viscosities significantly larger than those estimated from GRMHD simulations [75].

Turbulent angular momentum transport instead has a significant impact on the secondary features of the postmerger GW spectrum. In particular, we find that turbulence can shift and amplify secondary peaks in the spectrum that are formed at early time after merger [121]. Such features in the spectrum are analogous to those due to first order phase transitions [122]. Consequently, we caution that the search for new physics in the postmerger signal must account for the uncertainties related to the development of turbulence in the MNS. Follow up studies are necessary to precisely quantify them.

3.3. Outflows

Tidal interaction between the stars prior to merger and shocks after merger drive the ejection of neutron rich matter as the NSs coalesce [68,123]. In Ref. [88] we studied the impact of turbulent viscosity on the dynamical ejection of matter during BNS mergers. We found that turbulence can boost the ejection of matter in asymmetric binaries, but has only a small impact on the mass ejection from comparable mass binaries, such as the system considered in this study. Here, we confirm that these results hold also when using a calibrated turbulent viscosity model. In Fig. 5 we show the outflow rate of unbound matter (with $u_t \leq -1$) across a coordinate sphere with radius $R = 200 G/c^2 M_{\odot} \simeq 295$ km. The differences in the overall ejecta mass are not large, considering the large numerical uncertainties associated with the

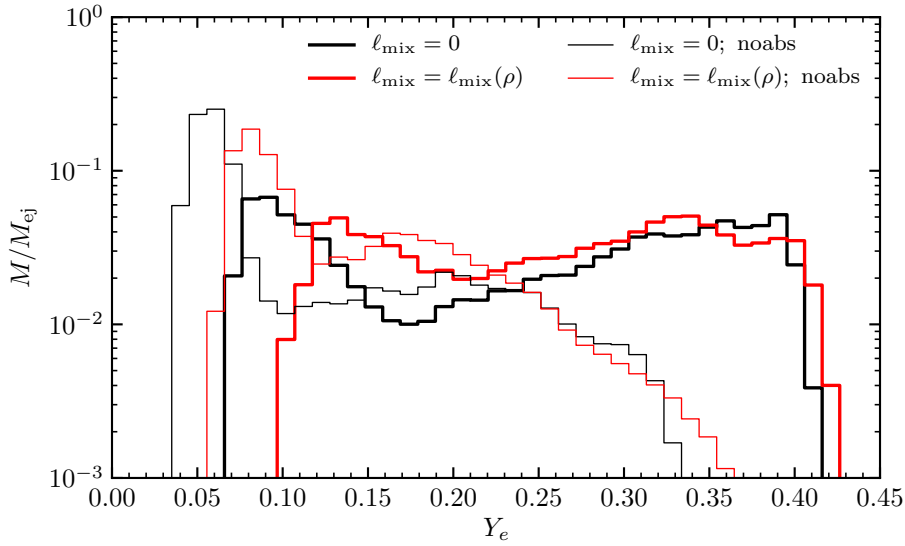


Figure 6. Histograms of the composition of the outflows from selected models. The thin lines denote simulations that did not include neutrino reabsorption. Turbulent viscosity and dissipation tend to increase the average electron fraction of the ejecta. However, this effect is subdominant compared to the effect of neutrino reabsorption.

calculation of the ejecta [58]. However, there is a clear trend in the outflow data. On the one hand, turbulent dissipation does not effect the outflow rate at early time, when fast material accelerated when the remnant rebounds reaches the detection sphere. On the other hand, the $\ell_{\text{mix}} > 0$ runs have significantly larger outflow rates at later times, when the slower part of the dynamical ejecta crosses the detection sphere. This is visible for the $\ell_{\text{mix}} = \ell_{\text{mix}}(\rho)$ simulations in Fig. 5. Simulations with other values of ℓ_{mix} follow the same trend, but are not included to avoid cluttering the figure. This late time boost of the outflow rate is likely the result of the increased thermalization of the flow due to turbulent viscosity and the resulting larger pressure gradients.

The effect of turbulent viscosity is, however, subdominant compared to the influence of neutrino reabsorption, which are found to play a key role in driving the “second wave” of the dynamical ejecta. Indeed, as shown in Fig. 5, this part of the outflow is almost completely absent when neutrino reabsorption is switched off in the simulations. This second component of the dynamical ejecta is predominantly constitute of neutrino-irradiated material at high latitudes above the merger remnant.

Both viscosity and neutrino reabsorption play an important role in the determination of the electron fraction Y_e of the ejecta [48–50,55,58], as shown in Fig. 6. This quantity is of particular interest since it most directly determines the outcomes of the r-process nucleosynthesis for the thermodynamic conditions typical of NS merger ejecta [124]. Turbulent dissipation increases the temperatures in the outflows activating pair capture processes which drive Y_e to higher values through the reaction $e^+ + n \rightarrow p + \bar{\nu}_e$. This effect is particularly pronounced when considering the tidal tail, which corresponds to the low- Y_e peak in the outflow distribution. Neutrino absorption has an even larger effect via the reaction $\nu_e + n \rightarrow p + e^-$. Neutrinos generate relatively high Y_e ejecta, especially at high latitudes [50]. They also effect the tidal tail, which is irradiated after colliding with the faster shock-accelerated outflows that are launched after the merger [58].

Turbulent angular momentum transport in the remnant accretion disk and neutrino heating are expected to power additional outflows on a timescale of a few seconds [47,56,57,61,62,125–132]. These

secular ejecta are expected to dominate the overall nucleosynthesis and electromagnetic signal from BNS mergers [58,133]. We considered the role of turbulent viscosity on the long term mass ejection in Ref. [61]. However, due to the large computational costs, we could not systematically vary ℓ_{mix} in Ref. [61]. Unfortunately, the simulations we present here do not span a sufficiently long time to be able to study the secular ejecta, so we leave this investigation to future work.

4. Discussion

MHD instabilities active in BNS merger remnants drive turbulence at many different scales [74,75]. Turbulence can generate large scale magnetic fields with potentially dramatic consequences for the evolution of the MNS remnants and its EM emissions [65,71,79]. Due to the large Reynolds number in the flow, directly capturing all scales of the turbulent flow in the MNS is beyond the reach of numerical simulations for the foreseeable future.

In Ref. [81] we proposed a scheme to include subgrid scale turbulence effects into global simulations and study the associated uncertainties on the multimessenger signatures of BNS mergers. Our method extends the LES methodology to GR. We derived evolution equations for coarse-grained fluid number, momentum, and energy densities. These equations are exact, but are not closed, so a closure must be provided. This closure represents the effect of small scale (subgrid) turbulence on the evolution of the large scale quantities. Here, we proposed to use a closure based on the classical turbulent viscosity ansatz [107], which we calibrated against very-high-resolution GRMHD simulations from Ref. [75]. We performed BNS merger simulations with microphysics and neutrinos using the newly proposed turbulence model. We showed that our scheme is robust and gives sensible results. We compared simulations performed with the newly calibrated scheme with simulations performed either with no subgrid model, or with a simpler scheme in which turbulent viscosity is assumed to be a constant fixed on the basis of dimensional analysis arguments.

Our results show that subgrid turbulence has a quantitative impact on the evolution of the remnant. Turbulence can affect the lifetime of the remnant, although large differences in the postmerger evolution are only found for values of the turbulent viscosity that are significantly larger than those found in GRMHD simulations. The peak frequency of the postmerger GW spectrum is found to be insensitive to turbulence, but secondary features in the spectrum and the overall luminosity in the postmerger are affected by turbulent dissipation. Turbulent angular momentum transport and dissipation alter the structure and composition of the remnant disk and the amount and composition of the dynamical ejecta, potentially impacting r-process nucleosynthesis yields and EM counterparts. However, turbulence is found to be subdominant when compared to neutrino effects.

More simulations are needed to establish the degree to which systematic uncertainties due to turbulence will limit our ability to search for new physics, such as phase transitions, in multimessenger observations of BNS mergers. The method we propose here can be and has been extended to the full-GRMHD equations [84,85]. Including GRMHD in our simulations is crucial to capture also the large scale effects due magnetic fields, such as jet launching [37,65], which are presently not included. In parallel, local high-resolution simulations should be performed to develop and calibrate turbulence models. These are all objectives of our future work.

Funding: This research used resources of the National Energy Research Scientific Computing Center, a DOE Office of Science User Facility supported by the Office of Science of the U.S. Department of Energy under Contract No. DE-AC02-05CH11231. Simulations were also performed on the supercomputers Comet and Stampede (NSF XSEDE allocation TG-PHY160025), on NSF/NCSA Blue Waters (NSF AWD-1811236), and on the Advanced Computer Infrastructure (ACI) of the Institute for Computational and Data Science (ICDS) at the Pennsylvania State University.

Acknowledgments: It is a pleasure to thank S. Bernuzzi for discussions that motivated this work, A. Prakash for carefully proofreading the manuscript, L. Weih and L. Rezzolla for discussions, and S. Hild for the ET-D noise curve data.

Conflicts of Interest: The author declares no conflict of interest.

References

1. Aasi, J.; others. Advanced LIGO. *Class. Quant. Grav.* **2015**, *32*, 074001, [arXiv:gr-qc/1411.4547]. doi:10.1088/0264-9381/32/7/074001.
2. Acernese, F.; others. Advanced Virgo: a second-generation interferometric gravitational wave detector. *Class. Quant. Grav.* **2015**, *32*, 024001, [arXiv:gr-qc/1408.3978]. doi:10.1088/0264-9381/32/2/024001.
3. Aso, Y.; Michimura, Y.; Somiya, K.; Ando, M.; Miyakawa, O.; Sekiguchi, T.; Tatsumi, D.; Yamamoto, H. Interferometer design of the KAGRA gravitational wave detector. *Phys. Rev.* **2013**, *D88*, 043007, [arXiv:gr-qc/1306.6747]. doi:10.1103/PhysRevD.88.043007.
4. Eichler, D.; Livio, M.; Piran, T.; Schramm, D.N. Nucleosynthesis, Neutrino Bursts and Gamma-Rays from Coalescing Neutron Stars. *Nature* **1989**, *340*, 126–128. doi:10.1038/340126a0.
5. Narayan, R.; Paczynski, B.; Piran, T. Gamma-ray bursts as the death throes of massive binary stars. *Astrophys. J.* **1992**, *395*, L83–L86, [arXiv:astro-ph/astro-ph/9204001]. doi:10.1086/186493.
6. Berger, E. Short-Duration Gamma-Ray Bursts. *Ann. Rev. Astron. Astrophys.* **2014**, *52*, 43–105, [arXiv:astro-ph.HE/1311.2603]. doi:10.1146/annurev-astro-081913-035926.
7. Kumar, P.; Zhang, B. The physics of gamma-ray bursts & relativistic jets. *Phys. Rept.* **2014**, *561*, 1–109, [arXiv:astro-ph.HE/1410.0679]. doi:10.1016/j.physrep.2014.09.008.
8. Fernández, R.; Metzger, B.D. Electromagnetic Signatures of Neutron Star Mergers in the Advanced LIGO Era. *Ann. Rev. Nucl. Part. Sci.* **2016**, *66*, 23–45, [arXiv:astro-ph.HE/1512.05435]. doi:10.1146/annurev-nucl-102115-044819.
9. Metzger, B.D. Kilonovae. *Living Rev. Rel.* **2020**, *23*, 1, [arXiv:astro-ph.HE/1910.01617]. doi:10.1007/s41114-019-0024-0.
10. Nakar, E. The electromagnetic counterparts of compact binary mergers **2019**. [arXiv:astro-ph.HE/1912.05659].
11. Abbott, B.P.; others. GW170817: Observation of Gravitational Waves from a Binary Neutron Star Inspiral. *Phys. Rev. Lett.* **2017**, *119*, 161101, [arXiv:gr-qc/1710.05832]. doi:10.1103/PhysRevLett.119.161101.
12. Abbott, B.P.; others. Properties of the binary neutron star merger GW170817. *Phys. Rev.* **2019**, *X9*, 011001, [arXiv:gr-qc/1805.11579]. doi:10.1103/PhysRevX.9.011001.
13. Wanajo, S.; Sekiguchi, Y.; Nishimura, N.; Kiuchi, K.; Kyutoku, K.; Shibata, M. Production of all the *r*-process nuclides in the dynamical ejecta of neutron star mergers. *Astrophys. J.* **2014**, *789*, L39, [arXiv:astro-ph.SR/1402.7317]. doi:10.1088/2041-8205/789/2/L39.
14. Hotokezaka, K.; Beniamini, P.; Piran, T. Neutron Star Mergers as sites of *r*-process Nucleosynthesis and Short Gamma-Ray Bursts. *Int. J. Mod. Phys.* **2018**, *D27*, 1842005, [arXiv:astro-ph.HE/1801.01141]. doi:10.1142/S0218271818420051.
15. Cowan, J.J.; Sneden, C.; Lawler, J.E.; Aprahamian, A.; Wiescher, M.; Langanke, K.; Martínez-Pinedo, G.; Thielemann, F.K. Origin of the Heaviest Elements: the Rapid Neutron-Capture Process **2019**. [arXiv:astro-ph.HE/1901.01410].
16. Abbott, B.P.; others. GW190425: Observation of a Compact Binary Coalescence with Total Mass $\sim 3.4M_{\odot}$. *Astrophys. J. Lett.* **2020**, *892*, L3, [arXiv:astro-ph.HE/2001.01761]. doi:10.3847/2041-8213/ab75f5.
17. Foley, R.J.; Coulter, D.A.; Kilpatrick, C.D.; Piro, A.L.; Ramirez-Ruiz, E.; Schwab, J. Updated Parameter Estimates for GW190425 Using Astrophysical Arguments and Implications for the Electromagnetic Counterpart. *Mon. Not. Roy. Astron. Soc.* **2020**, *494*, 190–198, [arXiv:astro-ph.HE/2002.00956]. doi:10.1093/mnras/staa725.
18. LIGO-Virgo Scientific Collaboration, Gravitational-Wave Candidate Event Database.

19. Abbott, B.P.; others. Prospects for Observing and Localizing Gravitational-Wave Transients with Advanced LIGO, Advanced Virgo and KAGRA. *Living Rev. Rel.* **2018**, *21*, 3, [arXiv:gr-qc/1304.0670]. doi:10.1007/s41114-018-0012-9, 10.1007/lrr-2016-1.
20. Hinderer, T. Tidal Love numbers of neutron stars. *Astrophys. J.* **2008**, *677*, 1216–1220, [arXiv:astro-ph/0711.2420]. doi:10.1086/533487.
21. Damour, T.; Nagar, A. Relativistic tidal properties of neutron stars. *Phys. Rev.* **2009**, *D80*, 084035, [arXiv:gr-qc/0906.0096]. doi:10.1103/PhysRevD.80.084035.
22. Damour, T.; Nagar, A.; Villain, L. Measurability of the tidal polarizability of neutron stars in late-inspiral gravitational-wave signals. *Phys. Rev.* **2012**, *D85*, 123007, [arXiv:gr-qc/1203.4352]. doi:10.1103/PhysRevD.85.123007.
23. Margalit, B.; Metzger, B.D. Constraining the Maximum Mass of Neutron Stars From Multi-Messenger Observations of GW170817. *Astrophys. J. Lett.* **2017**, *850*, L19, [arXiv:astro-ph.HE/1710.05938]. doi:10.3847/2041-8213/aa991c.
24. Annala, E.; Gorda, T.; Kurkela, A.; Vuorinen, A. Gravitational-wave constraints on the neutron-star-matter Equation of State. *Phys. Rev. Lett.* **2018**, *120*, 172703, [arXiv:astro-ph.HE/1711.02644]. doi:10.1103/PhysRevLett.120.172703.
25. De, S.; Finstad, D.; Lattimer, J.M.; Brown, D.A.; Berger, E.; Biwer, C.M. Tidal Deformabilities and Radii of Neutron Stars from the Observation of GW170817. *Phys. Rev. Lett.* **2018**, *121*, 091102, [arXiv:astro-ph.HE/1804.08583]. [Erratum: *Phys. Rev. Lett.* 121, no.25, 259902(2018)], doi:10.1103/PhysRevLett.121.259902, 10.1103/PhysRevLett.121.091102.
26. Ruiz, M.; Shapiro, S.L.; Tsokaros, A. GW170817, General Relativistic Magnetohydrodynamic Simulations, and the Neutron Star Maximum Mass. *Phys. Rev.* **2018**, *D97*, 021501, [arXiv:astro-ph.HE/1711.00473]. doi:10.1103/PhysRevD.97.021501.
27. Bauswein, A.; Just, O.; Janka, H.T.; Stergioulas, N. Neutron-star radius constraints from GW170817 and future detections. *Astrophys. J. Lett.* **2017**, *850*, L34, [arXiv:astro-ph.HE/1710.06843]. doi:10.3847/2041-8213/aa9994.
28. Radice, D.; Perego, A.; Zappa, F.; Bernuzzi, S. GW170817: Joint Constraint on the Neutron Star Equation of State from Multimessenger Observations. *Astrophys. J. Lett.* **2018**, *852*, L29, [arXiv:astro-ph.HE/1711.03647]. doi:10.3847/2041-8213/aaa402.
29. Most, E.R.; Weih, L.R.; Rezzolla, L.; Schaffner-Bielich, J. New constraints on radii and tidal deformabilities of neutron stars from GW170817. *Phys. Rev. Lett.* **2018**, *120*, 261103, [arXiv:gr-qc/1803.00549]. doi:10.1103/PhysRevLett.120.261103.
30. Tews, I.; Margueron, J.; Reddy, S. Critical examination of constraints on the equation of state of dense matter obtained from GW170817. *Phys. Rev. C* **2018**, *98*, 045804, [arXiv:nucl-th/1804.02783]. doi:10.1103/PhysRevC.98.045804.
31. Radice, D.; Dai, L. Multimessenger Parameter Estimation of GW170817. *Eur. Phys. J.* **2019**, *A55*, 50, [arXiv:astro-ph.HE/1810.12917]. doi:10.1140/epja/i2019-12716-4.
32. Kiuchi, K.; Kyutoku, K.; Shibata, M.; Taniguchi, K. Revisiting the lower bound on tidal deformability derived by AT 2017gfo. *Astrophys. J. Lett.* **2019**, *876*, L31, [arXiv:astro-ph.HE/1903.01466]. doi:10.3847/2041-8213/ab1e45.
33. Shibata, M.; Zhou, E.; Kiuchi, K.; Fujibayashi, S. Constraint on the maximum mass of neutron stars using GW170817 event. *Phys. Rev.* **2019**, *D100*, 023015, [arXiv:astro-ph.HE/1905.03656]. doi:10.1103/PhysRevD.100.023015.
34. Capano, C.D.; Tews, I.; Brown, S.M.; Margalit, B.; De, S.; Kumar, S.; Brown, D.A.; Krishnan, B.; Reddy, S. Stringent constraints on neutron-star radii from multimessenger observations and nuclear theory **2019**. [arXiv:astro-ph.HE/1908.10352]. doi:10.1038/s41550-020-1014-6.
35. Annala, E.; Gorda, T.; Kurkela, A.; Nättilä, J.; Vuorinen, A. Quark-matter cores in neutron stars **2019**. [arXiv:astro-ph.HE/1903.09121].
36. Dietrich, T.; Coughlin, M.W.; Pang, P.T.H.; Bulla, M.; Heinzl, J.; Issa, L.; Tews, I.; Antier, S. New Constraints on the Supranuclear Equation of State and the Hubble Constant from Nuclear Physics – Multi-Messenger Astronomy **2020**. [arXiv:astro-ph.HE/2002.11355].

37. Ruiz, M.; Lang, R.N.; Paschalidis, V.; Shapiro, S.L. Binary Neutron Star Mergers: a jet Engine for Short Gamma-ray Bursts. *Astrophys. J. Lett.* **2016**, *824*, L6, [[arXiv:astro-ph.HE/1604.02455](#)]. doi:10.3847/2041-8205/824/1/L6.
38. Abbott, B.P.; others. Gravitational Waves and Gamma-rays from a Binary Neutron Star Merger: GW170817 and GRB 170817A. *Astrophys. J. Lett.* **2017**, *848*, L13, [[arXiv:astro-ph.HE/1710.05834](#)]. doi:10.3847/2041-8213/aa920c.
39. Lazzati, D.; Perna, R.; Morsony, B.J.; López-Cámara, D.; Cantiello, M.; Ciolfi, R.; Giacomazzo, B.; Workman, J.C. Late time afterglow observations reveal a collimated relativistic jet in the ejecta of the binary neutron star merger GW170817. *Phys. Rev. Lett.* **2018**, *120*, 241103, [[arXiv:astro-ph.HE/1712.03237](#)]. doi:10.1103/PhysRevLett.120.241103.
40. Xie, X.; Zrake, J.; MacFadyen, A. Numerical Simulations of the Jet Dynamics and Synchrotron Radiation of Binary Neutron Star Merger Event GW170817/GRB 170817A. *Astrophys. J.* **2018**, *863*, 58, [[arXiv:astro-ph.HE/1804.09345](#)]. doi:10.3847/1538-4357/aac9c.
41. Hajela, A.; others. Two Years of Nonthermal Emission from the Binary Neutron Star Merger GW170817: Rapid Fading of the Jet Afterglow and First Constraints on the Kilonova Fastest Ejecta. *Astrophys. J. Lett.* **2019**, *886*, L17, [[arXiv:astro-ph.HE/1909.06393](#)]. doi:10.3847/2041-8213/ab5226.
42. Lazzati, D.; Ciolfi, R.; Perna, R. Intrinsic properties of the engine and jet that powered the short gamma-ray burst associated with GW170817 **2020**. [[arXiv:astro-ph.HE/2004.10210](#)].
43. Rosswog, S.; Liebendoerfer, M.; Thielemann, F.K.; Davies, M.B.; Benz, W.; Piran, T. Mass ejection in neutron star mergers. *Astron. Astrophys.* **1999**, *341*, 499–526, [[arXiv:astro-ph/astro-ph/9811367](#)].
44. Lee, W.H.; Ramirez-Ruiz, E.; Lopez-Camara, D. Phase transitions and He-synthesis driven winds in neutrino cooled accretion disks: prospects for late flares in short gamma-ray bursts. *Astrophys. J.* **2009**, *699*, L93–L96, [[arXiv:astro-ph.HE/0904.3752](#)]. doi:10.1088/0004-637X/699/2/L93.
45. Hotokezaka, K.; Kiuchi, K.; Kyutoku, K.; Okawa, H.; Sekiguchi, Y.i.; Shibata, M.; Taniguchi, K. Mass ejection from the merger of binary neutron stars. *Phys. Rev.* **2013**, *D87*, 024001, [[arXiv:astro-ph.HE/1212.0905](#)]. doi:10.1103/PhysRevD.87.024001.
46. Bauswein, A.; Goriely, S.; Janka, H.T. Systematics of dynamical mass ejection, nucleosynthesis, and radioactively powered electromagnetic signals from neutron-star mergers. *Astrophys. J.* **2013**, *773*, 78, [[arXiv:astro-ph.SR/1302.6530](#)]. doi:10.1088/0004-637X/773/1/78.
47. Perego, A.; Rosswog, S.; Cabezón, R.M.; Korobkin, O.; Käppeli, R.; Arcones, A.; Liebendörfer, M. Neutrino-driven winds from neutron star merger remnants. *Mon. Not. Roy. Astron. Soc.* **2014**, *443*, 3134–3156, [[arXiv:astro-ph.HE/1405.6730](#)]. doi:10.1093/mnras/stu1352.
48. Sekiguchi, Y.; Kiuchi, K.; Kyutoku, K.; Shibata, M.; Taniguchi, K. Dynamical mass ejection from the merger of asymmetric binary neutron stars: Radiation-hydrodynamics study in general relativity. *Phys. Rev.* **2016**, *D93*, 124046, [[arXiv:astro-ph.HE/1603.01918](#)]. doi:10.1103/PhysRevD.93.124046.
49. Foucart, F.; Haas, R.; Duez, M.D.; O'Connor, E.; Ott, C.D.; Roberts, L.; Kidder, L.E.; Lippuner, J.; Pfeiffer, H.P.; Scheel, M.A. Low mass binary neutron star mergers : gravitational waves and neutrino emission. *Phys. Rev.* **2016**, *D93*, 044019, [[arXiv:astro-ph.HE/1510.06398](#)]. doi:10.1103/PhysRevD.93.044019.
50. Radice, D.; Galeazzi, F.; Lippuner, J.; Roberts, L.F.; Ott, C.D.; Rezzolla, L. Dynamical Mass Ejection from Binary Neutron Star Mergers. *Mon. Not. Roy. Astron. Soc.* **2016**, *460*, 3255–3271, [[arXiv:astro-ph.HE/1601.02426](#)]. doi:10.1093/mnras/stw1227.
51. Lehner, L.; Liebling, S.L.; Palenzuela, C.; Caballero, O.L.; O'Connor, E.; Anderson, M.; Neilsen, D. Unequal mass binary neutron star mergers and multimessenger signals. *Class. Quant. Grav.* **2016**, *33*, 184002, [[arXiv:gr-qc/1603.00501](#)]. doi:10.1088/0264-9381/33/18/184002.
52. Dietrich, T.; Ujevic, M.; Tichy, W.; Bernuzzi, S.; Bruegmann, B. Gravitational waves and mass ejecta from binary neutron star mergers: Effect of the mass-ratio. *Phys. Rev.* **2017**, *D95*, 024029, [[arXiv:gr-qc/1607.06636](#)]. doi:10.1103/PhysRevD.95.024029.
53. Siegel, D.M.; Metzger, B.D. Three-Dimensional General-Relativistic Magnetohydrodynamic Simulations of Remnant Accretion Disks from Neutron Star Mergers: Outflows and *r*-Process Nucleosynthesis. *Phys. Rev. Lett.* **2017**, *119*, 231102, [[arXiv:astro-ph.HE/1705.05473](#)]. doi:10.1103/PhysRevLett.119.231102.

54. Kasen, D.; Metzger, B.; Barnes, J.; Quataert, E.; Ramirez-Ruiz, E. Origin of the heavy elements in binary neutron-star mergers from a gravitational wave event. *Nature* **2017**, [arXiv:astro-ph.HE/1710.05463]. [Nature551,80(2017)], doi:10.1038/nature24453.
55. Foucart, F.; O'Connor, E.; Roberts, L.; Kidder, L.E.; Pfeiffer, H.P.; Scheel, M.A. Impact of an improved neutrino energy estimate on outflows in neutron star merger simulations. *Phys. Rev.* **2016**, *D94*, 123016, [arXiv:astro-ph.HE/1607.07450]. doi:10.1103/PhysRevD.94.123016.
56. Fujibayashi, S.; Kiuchi, K.; Nishimura, N.; Sekiguchi, Y.; Shibata, M. Mass Ejection from the Remnant of a Binary Neutron Star Merger: Viscous-Radiation Hydrodynamics Study. *Astrophys. J.* **2018**, *860*, 64, [arXiv:astro-ph.HE/1711.02093]. doi:10.3847/1538-4357/aabafd.
57. Fernández, R.; Tchekhovskoy, A.; Quataert, E.; Foucart, F.; Kasen, D. Long-term GRMHD simulations of neutron star merger accretion discs: implications for electromagnetic counterparts. *Mon. Not. Roy. Astron. Soc.* **2019**, *482*, 3373–3393, [arXiv:astro-ph.HE/1808.00461]. doi:10.1093/mnras/sty2932.
58. Radice, D.; Perego, A.; Hotokezaka, K.; Fromm, S.A.; Bernuzzi, S.; Roberts, L.F. Binary Neutron Star Mergers: Mass Ejection, Electromagnetic Counterparts and Nucleosynthesis. *Astrophys. J.* **2018**, *869*, 130, [arXiv:astro-ph.HE/1809.11161]. doi:10.3847/1538-4357/aaf054.
59. Miller, J.M.; Ryan, B.R.; Dolence, J.C.; Burrows, A.; Fontes, C.J.; Fryer, C.L.; Korobkin, O.; Lippuner, J.; Mumpower, M.R.; Wollaeger, R.T. Full Transport Model of GW170817-Like Disk Produces a Blue Kilonova. *Phys. Rev.* **2019**, *D100*, 023008, [arXiv:astro-ph.HE/1905.07477]. doi:10.1103/PhysRevD.100.023008.
60. Vincent, T.; Foucart, F.; Duez, M.D.; Haas, R.; Kidder, L.E.; Pfeiffer, H.P.; Scheel, M.A. Unequal Mass Binary Neutron Star Simulations with Neutrino Transport: Ejecta and Neutrino Emission. *Phys. Rev.* **2020**, *D101*, 044053, [arXiv:gr-qc/1908.00655]. doi:10.1103/PhysRevD.101.044053.
61. Nedora, V.; Bernuzzi, S.; Radice, D.; Perego, A.; Endrizzi, A.; Ortiz, N. Spiral-wave wind for the blue kilonova. *Astrophys. J. Lett.* **2019**, *886*, L30, [arXiv:astro-ph.HE/1907.04872]. doi:10.3847/2041-8213/ab5794.
62. Fujibayashi, S.; Shibata, M.; Wanajo, S.; Kiuchi, K.; Kyutoku, K.; Sekiguchi, Y. Mass ejection from disks surrounding a low-mass black hole: Viscous neutrino-radiation hydrodynamics simulation in full general relativity. *Phys. Rev.* **2020**, *D101*, 083029, [arXiv:astro-ph.HE/2001.04467]. doi:10.1103/PhysRevD.101.083029.
63. Palenzuela, C.; Liebling, S.L.; Neilsen, D.; Lehner, L.; Caballero, O.L.; O'Connor, E.; Anderson, M. Effects of the microphysical Equation of State in the mergers of magnetized Neutron Stars With Neutrino Cooling. *Phys. Rev.* **2015**, *D92*, 044045, [arXiv:gr-qc/1505.01607]. doi:10.1103/PhysRevD.92.044045.
64. Most, E.R.; Papenfort, L.J.; Rezzolla, L. Beyond second-order convergence in simulations of magnetized binary neutron stars with realistic microphysics. *Mon. Not. Roy. Astron. Soc.* **2019**, *490*, 3588–3600, [arXiv:astro-ph.HE/1907.10328]. doi:10.1093/mnras/stz2809.
65. Mösta, P.; Radice, D.; Haas, R.; Schnetter, E.; Bernuzzi, S. A magnetar engine for short GRBs and kilonovae **2020**. [arXiv:astro-ph.HE/2003.06043].
66. Jesse, J.; Duez, M.D.; Foucart, F.; Haddadi, M.; Knight, A.L.; Cadenhead, C.L.; Hébert, F.; Kidder, L.E.; Pfeiffer, H.P.; Scheel, M.A. Axisymmetric Hydrodynamics in Numerical Relativity Using a Multipatch Method **2020**. [arXiv:gr-qc/2005.01848].
67. Radice, D.; Perego, A.; Bernuzzi, S.; Zhang, B. Long-lived Remnants from Binary Neutron Star Mergers. *Mon. Not. Roy. Astron. Soc.* **2018**, *481*, 3670–3682, [arXiv:astro-ph.HE/1803.10865]. doi:10.1093/mnras/sty2531.
68. Radice, D.; Bernuzzi, S.; Perego, A. The Dynamics of Binary Neutron Star Mergers and of GW170817 **2020**. [arXiv:astro-ph.HE/2002.03863]. doi:10.1146/annurev-nucl-013120-114541.
69. Obergaulinger, M.; Aloy, M.A.; Müller, E. Local simulations of the magnetized Kelvin-Helmholtz instability in neutron-star mergers. *Astron. Astrophys.* **2010**, *515*, A30, [arXiv:astro-ph.SR/1003.6031]. doi:10.1051/0004-6361/200913386.
70. Bucciantini, N.; Metzger, B.D.; Thompson, T.A.; Quataert, E. Short GRBs with Extended Emission from Magnetar Birth: Jet Formation and Collimation. *Mon. Not. Roy. Astron. Soc.* **2012**, *419*, 1537, [arXiv:astro-ph.HE/1106.4668]. doi:10.1111/j.1365-2966.2011.19810.x.
71. Siegel, D.M.; Ciolfi, R.; Harte, A.I.; Rezzolla, L. Magnetorotational instability in relativistic hypermassive neutron stars. *Phys. Rev.* **2013**, *D87*, 121302, [arXiv:gr-qc/1302.4368]. doi:10.1103/PhysRevD.87.121302.

72. Kiuchi, K.; Kyutoku, K.; Sekiguchi, Y.; Shibata, M.; Wada, T. High resolution numerical-relativity simulations for the merger of binary magnetized neutron stars. *Phys. Rev.* **2014**, *D90*, 041502, [[arXiv:astro-ph.HE/1407.2660](#)]. doi:10.1103/PhysRevD.90.041502.
73. Giacomazzo, B.; Zrake, J.; Duffell, P.; MacFadyen, A.I.; Perna, R. Producing Magnetar Magnetic Fields in the Merger of Binary Neutron Stars. *Astrophys. J.* **2015**, *809*, 39, [[arXiv:astro-ph.HE/1410.0013](#)]. doi:10.1088/0004-637X/809/1/39.
74. Kiuchi, K.; Cerdá-Durán, P.; Kyutoku, K.; Sekiguchi, Y.; Shibata, M. Efficient magnetic-field amplification due to the Kelvin-Helmholtz instability in binary neutron star mergers. *Phys. Rev.* **2015**, *D92*, 124034, [[arXiv:astro-ph.HE/1509.09205](#)]. doi:10.1103/PhysRevD.92.124034.
75. Kiuchi, K.; Kyutoku, K.; Sekiguchi, Y.; Shibata, M. Global simulations of strongly magnetized remnant massive neutron stars formed in binary neutron star mergers. *Phys. Rev.* **2018**, *D97*, 124039, [[arXiv:astro-ph.HE/1710.01311](#)]. doi:10.1103/PhysRevD.97.124039.
76. Duez, M.D.; Liu, Y.T.; Shapiro, S.L.; Stephens, B.C. General relativistic hydrodynamics with viscosity: Contraction, catastrophic collapse, and disk formation in hypermassive neutron stars. *Phys. Rev.* **2004**, *D69*, 104030, [[arXiv:astro-ph/astro-ph/0402502](#)]. doi:10.1103/PhysRevD.69.104030.
77. Duez, M.D.; Liu, Y.T.; Shapiro, S.L.; Shibata, M. Evolution of magnetized, differentially rotating neutron stars: Simulations in full general relativity. *Phys. Rev.* **2006**, *D73*, 104015, [[arXiv:astro-ph/astro-ph/0605331](#)]. doi:10.1103/PhysRevD.73.104015.
78. Hotokezaka, K.; Kiuchi, K.; Kyutoku, K.; Muranushi, T.; Sekiguchi, Y.i.; Shibata, M.; Taniguchi, K. Remnant massive neutron stars of binary neutron star mergers: Evolution process and gravitational waveform. *Phys. Rev.* **2013**, *D88*, 044026, [[arXiv:astro-ph.HE/1307.5888](#)]. doi:10.1103/PhysRevD.88.044026.
79. Ciolfi, R.; Kastaun, W.; Kalinani, J.V.; Giacomazzo, B. First 100 ms of a long-lived magnetized neutron star formed in a binary neutron star merger. *Phys. Rev.* **2019**, *D100*, 023005, [[arXiv:astro-ph.HE/1904.10222](#)]. doi:10.1103/PhysRevD.100.023005.
80. Guilet, J.; Bauswein, A.; Just, O.; Janka, H.T. Magnetorotational instability in neutron star mergers: impact of neutrinos. *Mon. Not. Roy. Astron. Soc.* **2017**, *471*, 1879–1887, [[arXiv:astro-ph.HE/1610.08532](#)]. doi:10.1093/mnras/stx1739.
81. Radice, D. General-Relativistic Large-Eddy Simulations of Binary Neutron Star Mergers. *Astrophys. J.* **2017**, *838*, L2, [[arXiv:astro-ph.HE/1703.02046](#)]. doi:10.3847/2041-8213/aa6483.
82. Shibata, M.; Kiuchi, K.; Sekiguchi, Y.i. General relativistic viscous hydrodynamics of differentially rotating neutron stars. *Phys. Rev.* **2017**, *D95*, 083005, [[arXiv:astro-ph.HE/1703.10303](#)]. doi:10.1103/PhysRevD.95.083005.
83. Eyink, G.L.; Drivas, T.D. Cascades and Dissipative Anomalies in Relativistic Fluid Turbulence. *Phys. Rev.* **2018**, *X8*, 011023, [[arXiv:physics.flu-dyn/1704.03541](#)]. doi:10.1103/PhysRevX.8.011023.
84. Carrasco, F.; Viganò, D.; Palenzuela, C. Gradient subgrid-scale model for relativistic MHD large-eddy simulations. *Phys. Rev.* **2020**, *D101*, 063003, [[arXiv:astro-ph.HE/1908.01419](#)]. doi:10.1103/PhysRevD.101.063003.
85. Viganò, D.; Aguilera-Miret, R.; Carrasco, F.; Miñano, B.; Palenzuela, C. GRMHD large eddy simulations with gradient subgrid-scale model **2020**. [[arXiv:gr-qc/2004.00870](#)].
86. Rosofsky, S.G.; Huerta, E.A. Artificial neural network subgrid models of 2D compressible magnetohydrodynamic turbulence. *Phys. Rev.* **2020**, *D101*, 084024, [[arXiv:physics.comp-ph/1912.11073](#)]. doi:10.1103/PhysRevD.101.084024.
87. Zappa, F.; Bernuzzi, S.; Radice, D.; Perego, A.; Dietrich, T. Gravitational-wave luminosity of binary neutron star mergers. *Phys. Rev. Lett.* **2018**, *120*, 111101, [[arXiv:gr-qc/1712.04267](#)]. doi:10.1103/PhysRevLett.120.111101.
88. Radice, D.; Perego, A.; Hotokezaka, K.; Bernuzzi, S.; Fromm, S.A.; Roberts, L.F. Viscous-Dynamical Ejecta from Binary Neutron Star Merger. *Astrophys. J. Lett.* **2018**, *869*, L35, [[arXiv:astro-ph.HE/1809.11163](#)]. doi:10.3847/2041-8213/aaf053.
89. Perego, A.; Bernuzzi, S.; Radice, D. Thermodynamics conditions of matter in neutron star mergers. *Eur. Phys. J.* **2019**, *A55*, 124, [[arXiv:gr-qc/1903.07898](#)]. doi:10.1140/epja/i2019-12810-7.

90. Bernuzzi, S.; others. Accretion-induced prompt black hole formation in asymmetric neutron star mergers, dynamical ejecta and kilonova signals **2020**. [[arXiv:astro-ph.HE/2003.06015](#)].
91. Radice, D.; Rezzolla, L. THC: a new high-order finite-difference high-resolution shock-capturing code for special-relativistic hydrodynamics. *Astron. Astrophys.* **2012**, *547*, A26, [[arXiv:astro-ph.IM/1206.6502](#)]. doi:10.1051/0004-6361/201219735.
92. Radice, D.; Rezzolla, L.; Galeazzi, F. Beyond second-order convergence in simulations of binary neutron stars in full general-relativity. *Mon. Not. Roy. Astron. Soc.* **2014**, *437*, L46–L50, [[arXiv:gr-qc/1306.6052](#)]. doi:10.1093/mnrasl/slt137.
93. Radice, D.; Rezzolla, L.; Galeazzi, F. High-Order Fully General-Relativistic Hydrodynamics: new Approaches and Tests. *Class. Quant. Grav.* **2014**, *31*, 075012, [[arXiv:gr-qc/1312.5004](#)]. doi:10.1088/0264-9381/31/7/075012.
94. Radice, D.; Rezzolla, L.; Galeazzi, F. High-Order Numerical-Relativity Simulations of Binary Neutron Stars. *ASP Conf. Ser.* **2015**, *498*, 121–126, [[arXiv:gr-qc/1502.00551](#)].
95. Bernuzzi, S.; Hilditch, D. Constraint violation in free evolution schemes: Comparing BSSNOK with a conformal decomposition of Z4. *Phys. Rev.* **2010**, *D81*, 084003, [[arXiv:gr-qc/0912.2920](#)]. doi:10.1103/PhysRevD.81.084003.
96. Hilditch, D.; Bernuzzi, S.; Thierfelder, M.; Cao, Z.; Tichy, W.; Bruegmann, B. Compact binary evolutions with the Z4c formulation. *Phys. Rev.* **2013**, *D88*, 084057, [[arXiv:gr-qc/1212.2901](#)]. doi:10.1103/PhysRevD.88.084057.
97. Pollney, D.; Reisswig, C.; Schnetter, E.; Dorband, N.; Diener, P. High accuracy binary black hole simulations with an extended wave zone. *Phys. Rev.* **2011**, *D83*, 044045, [[arXiv:gr-qc/0910.3803](#)]. doi:10.1103/PhysRevD.83.044045.
98. Reisswig, C.; Ott, C.D.; Abdikamalov, E.; Haas, R.; Moesta, P.; Schnetter, E. Formation and Coalescence of Cosmological Supermassive Black Hole Binaries in Supermassive Star Collapse. *Phys. Rev. Lett.* **2013**, *111*, 151101, [[arXiv:astro-ph.CO/1304.7787](#)]. doi:10.1103/PhysRevLett.111.151101.
99. Babiuc-Hamilton, M.; Brandt, S.R.; Diener, P.; Elley, M.; Etienne, Z.; Ficarra, G.; Haas, R.; Witek, H.; Alcubierre, M.; Alic, D.; Allen, G.; Ansorg, M.; Baiotti, L.; Bengert, W.; Bentivegna, E.; Bernuzzi, S.; Bode, T.; Bruegmann, B.; Corvino, G.; Pietri, R.D.; Dimmelmeier, H.; Rion Dooley.; Dorband, N.; Khamra, Y.E.; Faber, J.; Font, T.; Friebe, J.; Giacomazzo, B.; Goodale, T.; Gundlach, C.; Hawke, I.; Hawley, S.; Hinder, I.; Husa, S.; Iyer, S.; Kellermann, T.; Knapp, A.; Koppitz, M.; Lanferman, G.; Löffler, F.; Masso, J.; Menger, L.; Merzky, A.; Miller, M.; Moesta, P.; Montero, P.; Mundim, B.; Nerozzi, A.; Ott, C.; Paruchuri, R.; Pollney, D.; Radice, D.; Radke, T.; Reisswig, C.; Rezzolla, L.; Rideout, D.; Ripeanu, M.; Schnetter, E.; Schutz, B.; Seidel, E.; Seidel, E.; Shalf, J.; Spherhake, U.; Stergioulas, N.; Wai-Mo Suen.; Szilagy, B.; Takahashi, R.; Thomas, M.; Thornburg, J.; Tobias, M.; Aaryn Tonita.; Walker, P.; Mew-Bing Wan.; Wardell, B.; Zilhão, M.; Zink, B.; Zlochower, Y. The Einstein Toolkit, 2019. doi:10.5281/ZENODO.3522086.
100. Löffler, F.; others. The Einstein Toolkit: A Community Computational Infrastructure for Relativistic Astrophysics. *Class. Quant. Grav.* **2012**, *29*, 115001, [[arXiv:gr-qc/1111.3344](#)]. doi:10.1088/0264-9381/29/11/115001.
101. Gottlieb, S.; Ketcheson, D.I.; Shu, C.W. High Order Strong Stability Preserving Time Discretizations. *Journal of Scientific Computing* **2008**, *38*, 251–289. doi:10.1007/s10915-008-9239-z.
102. Schnetter, E.; Hawley, S.H.; Hawke, I. Evolutions in 3-D numerical relativity using fixed mesh refinement. *Class. Quant. Grav.* **2004**, *21*, 1465–1488, [[arXiv:gr-qc/gr-qc/0310042](#)]. doi:10.1088/0264-9381/21/6/014.
103. Berger, M.J.; Olinger, J. Adaptive Mesh Refinement for Hyperbolic Partial Differential Equations. *J. Comput. Phys.* **1984**, *53*, 484. doi:10.1016/0021-9991(84)90073-1.
104. Berger, M.J.; Colella, P. Local Adaptive Mesh Refinement for Shock Hydrodynamics. *Journal of Computational Physics* **1989**, *82*, 64–84. doi:10.1016/0021-9991(89)90035-1.
105. Reisswig, C.; Haas, R.; Ott, C.D.; Abdikamalov, E.; Mösta, P.; Pollney, D.; Schnetter, E. Three-Dimensional General-Relativistic Hydrodynamic Simulations of Binary Neutron Star Coalescence and Stellar Collapse with Multipatch Grids. *Phys. Rev.* **2013**, *D87*, 064023, [[arXiv:astro-ph.HE/1212.1191](#)]. doi:10.1103/PhysRevD.87.064023.
106. Banyuls, F.; Font, J.A.; Ibanez, J.M.A.; Martí, J.M.A.; Miralles, J.A. Numerical 3+1 General Relativistic Hydrodynamics: A Local Characteristic Approach. *Astrophys. J.* **1997**, *476*, 221.

107. Smagorinsky, J. GENERAL CIRCULATION EXPERIMENTS WITH THE PRIMITIVE EQUATIONS. *Monthly Weather Review* **1963**, *91*, 99–164. doi:10.1175/1520-0493(1963)091<0099:gcewtp>2.3.co;2.
108. Shakura, N.I.; Sunyaev, R.A. Reprint of 1973A&A....24..337S. Black holes in binary systems. Observational appearance. *Astro. Astrophys.* **1973**, *500*, 33–51.
109. Shibata, M.; Taniguchi, K.; Uryu, K. Merger of binary neutron stars with realistic equations of state in full general relativity. *Phys. Rev.* **2005**, *D71*, 084021, [arXiv:gr-qc/gr-qc/0503119]. doi:10.1103/PhysRevD.71.084021.
110. Kastaun, W.; Ciolfi, R.; Giacomazzo, B. Structure of Stable Binary Neutron Star Merger Remnants: a Case Study. *Phys. Rev.* **2016**, *D94*, 044060, [arXiv:astro-ph.HE/1607.02186]. doi:10.1103/PhysRevD.94.044060.
111. Hanauske, M.; Takami, K.; Bovard, L.; Rezzolla, L.; Font, J.A.; Galeazzi, F.; Stöcker, H. Rotational properties of hypermassive neutron stars from binary mergers. *Phys. Rev.* **2017**, *D96*, 043004, [arXiv:gr-qc/1611.07152]. doi:10.1103/PhysRevD.96.043004.
112. Ciolfi, R.; Kastaun, W.; Giacomazzo, B.; Endrizzi, A.; Siegel, D.M.; Perna, R. General relativistic magnetohydrodynamic simulations of binary neutron star mergers forming a long-lived neutron star. *Phys. Rev.* **2017**, *D95*, 063016, [arXiv:astro-ph.HE/1701.08738]. doi:10.1103/PhysRevD.95.063016.
113. Lattimer, J.M.; Swesty, F.D. A Generalized equation of state for hot, dense matter. *Nucl. Phys.* **1991**, *A535*, 331–376. doi:10.1016/0375-9474(91)90452-C.
114. Gourgoulhon, E.; Grandclément, P.; Marck, J.A.; Novak, J.; Taniguchi, K. LORENE, 1999. Paris Observatory, Meudon section - LUTH laboratory.
115. Bernuzzi, S.; Radice, D.; Ott, C.D.; Roberts, L.F.; Moesta, P.; Galeazzi, F. How loud are neutron star mergers? *Phys. Rev.* **2016**, *D94*, 024023, [arXiv:gr-qc/1512.06397]. doi:10.1103/PhysRevD.94.024023.
116. Bauswein, A.; Janka, H.T. Measuring neutron-star properties via gravitational waves from binary mergers. *Phys. Rev. Lett.* **2012**, *108*, 011101, [arXiv:astro-ph.SR/1106.1616]. doi:10.1103/PhysRevLett.108.011101.
117. Takami, K.; Rezzolla, L.; Baiotti, L. Constraining the Equation of State of Neutron Stars from Binary Mergers. *Phys. Rev. Lett.* **2014**, *113*, 091104, [arXiv:gr-qc/1403.5672]. doi:10.1103/PhysRevLett.113.091104.
118. Bernuzzi, S.; Dietrich, T.; Nagar, A. Modeling the complete gravitational wave spectrum of neutron star mergers. *Phys. Rev. Lett.* **2015**, *115*, 091101, [arXiv:gr-qc/1504.01764]. doi:10.1103/PhysRevLett.115.091101.
119. Breschi, M.; Bernuzzi, S.; Zappa, F.; Agathos, M.; Perego, A.; Radice, D.; Nagar, A. kiloHertz gravitational waves from binary neutron star remnants: time-domain model and constraints on extreme matter. *Phys. Rev.* **2019**, *D100*, 104029, [arXiv:gr-qc/1908.11418]. doi:10.1103/PhysRevD.100.104029.
120. Shibata, M.; Kiuchi, K. Gravitational waves from remnant massive neutron stars of binary neutron star merger: Viscous hydrodynamics effects. *Phys. Rev.* **2017**, *D95*, 123003, [arXiv:astro-ph.HE/1705.06142]. doi:10.1103/PhysRevD.95.123003.
121. Rezzolla, L.; Takami, K. Gravitational-wave signal from binary neutron stars: a systematic analysis of the spectral properties. *Phys. Rev.* **2016**, *D93*, 124051, [arXiv:gr-qc/1604.00246]. doi:10.1103/PhysRevD.93.124051.
122. Weih, L.R.; Hanauske, M.; Rezzolla, L. Postmerger Gravitational-Wave Signatures of Phase Transitions in Binary Mergers. *Phys. Rev. Lett.* **2020**, *124*, 171103, [arXiv:gr-qc/1912.09340]. doi:10.1103/PhysRevLett.124.171103.
123. Shibata, M.; Hotokezaka, K. Merger and Mass Ejection of Neutron-Star Binaries. *Ann. Rev. Nucl. Part. Sci.* **2019**, *69*, 41–64, [arXiv:astro-ph.HE/1908.02350]. doi:10.1146/annurev-nucl-101918-023625.
124. Lippuner, J.; Roberts, L.F. r-Process Lanthanide Production and Heating Rates in Kilonovae. *Astrophys. J.* **2015**, *815*, 82, [arXiv:astro-ph.HE/1508.03133]. doi:10.1088/0004-637X/815/2/82.
125. Metzger, B.D.; Piro, A.L.; Quataert, E. Time-Dependent Models of Accretion Disks Formed from Compact Object Mergers. *Mon. Not. Roy. Astron. Soc.* **2008**, *390*, 781, [arXiv:astro-ph/0805.4415]. doi:10.1111/j.1365-2966.2008.13789.x.
126. Metzger, B.D.; Piro, A.L.; Quataert, E. Neutron-Rich Freeze-Out in Viscously Spreading Accretion Disks Formed from Compact Object Mergers. *Mon. Not. Roy. Astron. Soc.* **2009**, *396*, 304, [arXiv:astro-ph/0810.2535]. doi:10.1111/j.1365-2966.2008.14380.x.
127. Lee, W.H.; Ramirez-Ruiz, E.; López-Cámara, D. Phase Transitions and He-Synthesis-Driven Winds in Neutrino Cooled Accretion Disks: Prospects for Late Flares in Short Gamma-Ray Bursts. *Astrophys. J. Lett* **2009**, *699*, L93–L96, [arXiv:astro-ph.HE/0904.3752]. doi:10.1088/0004-637X/699/2/L93.

128. Fernández, R.; Metzger, B.D. Delayed outflows from black hole accretion tori following neutron star binary coalescence. *Mon. Not. Roy. Astron. Soc.* **2013**, *435*, 502, [[arXiv:astro-ph.HE/1304.6720](#)]. doi:10.1093/mnras/stt1312.
129. Just, O.; Bauswein, A.; Pulpillo, R.A.; Goriely, S.; Janka, H.T. Comprehensive nucleosynthesis analysis for ejecta of compact binary mergers. *Mon. Not. Roy. Astron. Soc.* **2015**, *448*, 541–567, [[arXiv:astro-ph.SR/1406.2687](#)]. doi:10.1093/mnras/stv009.
130. Metzger, B.D.; Fernández, R. Red or blue? A potential kilonova imprint of the delay until black hole formation following a neutron star merger. *Mon. Not. Roy. Astron. Soc.* **2014**, *441*, 3444–3453, [[arXiv:astro-ph.HE/1402.4803](#)]. doi:10.1093/mnras/stu802.
131. Martin, D.; Perego, A.; Arcones, A.; Thielemann, F.K.; Korobkin, O.; Rosswog, S. Neutrino-driven winds in the aftermath of a neutron star merger: nucleosynthesis and electromagnetic transients. *Astrophys. J.* **2015**, *813*, 2, [[arXiv:astro-ph.SR/1506.05048](#)]. doi:10.1088/0004-637X/813/1/2.
132. Siegel, D.M.; Metzger, B.D. Three-dimensional GRMHD simulations of neutrino-cooled accretion disks from neutron star mergers. *Astrophys. J.* **2018**, *858*, 52, [[arXiv:astro-ph.HE/1711.00868](#)]. doi:10.3847/1538-4357/aabaec.
133. Siegel, D.M. GW170817—the first observed neutron star merger and its kilonova: implications for the astrophysical site of the r-process. *Eur. Phys. J.* **2019**, *A55*, 203, [[arXiv:astro-ph.HE/1901.09044](#)]. doi:10.1140/epja/i2019-12888-9.

© 2021 by the author. Submitted to *Symmetry* for possible open access publication under the terms and conditions of the Creative Commons Attribution (CC BY) license (<http://creativecommons.org/licenses/by/4.0/>).